Clim Dyn (2011) 36:945–955
DOI 10.1007/s00382-010-0756-8

Atmospheric inversion strength over polar oceans in winter regulated by sea ice

Tamlin M. Pavelsky · Julien Boé · Alex Hall · Eric J. Fetzer

Received: 9 July 2009 / Accepted: 27 January 2010 / Published online: 25 February 2010

Abstract Low-level temperature inversions are a common feature of the wintertime troposphere in the Arctic and Antarctic. Inversion strength plays an important role in regulating atmospheric processes including air pollution, ozone destruction, cloud formation, and negative longwave feedback mechanisms that shape polar climate response to anthropogenic forcing. The Atmospheric Infrared Sounder (AIRS) instrument provides reliable measures of spatial patterns in mean wintertime inversion strength when compared with available radiosonde observations and reanalysis products. Here, we examine the influence of sea ice concentration on inversion strength in the Arctic and Antarctic. Correlation of inversion strength with mean annual sea ice concentration, likely a surrogate for the effective thermal conductivity of the wintertime ice pack, yields strong, linear relationships in the Arctic ($r = 0.88$) and Antarctic ($r = 0.86$). We find a substantially greater (stronger) linear relationship between sea ice concentration and surface air temperature than with temperature at 850 hPa, lending credence to the idea that sea ice controls inversion strength through modulation of surface heat fluxes. As such, declines in sea ice in either hemisphere may imply weaker mean inversions in the future. Comparison of mean inversion strength in AIRS and global climate models (GCMs) suggests that many GCMs poorly characterize mean inversion strength at high latitudes.

Keywords Temperature inversion · Sea ice · Arctic · Antarctic · AIRS

T. M. Pavelsky (✉)
Department of Geological Sciences,
University of North Carolina, CB 3315,
Chapel Hill, NC 27599, USA
e-mail: pavelsky@unc.edu

J. Boé · A. Hall
Department of Atmospheric and Oceanic Sciences,
University of California Los Angeles, Box 951565,
Los Angeles, CA 90095, USA

E. J. Fetzer
Jet Propulsion Laboratory, California Institute of Technology,
M/S 169-237, 4800 Oak Grove Drive,
Pasadena, CA 91109, USA

1 Introduction

Low-level temperature inversions have long been recognized as a pervasive feature of the Arctic (Wexler 1936; Vowinkel and Orvig 1970; Curry et al. 1996) and Antarctic (Phillpot and Zillman 1970; Connolley 1996) atmospheres in winter. They arise from multiple sources including warm air advection and subsidence, though a deficit in net surface radiation is the most common cause (Serreze et al. 1992; Liu et al. 2006). Inversion strength and depth regulate processes central to polar climate, including the depth of the atmospheric mixed layer and transport of heat and moisture from leads and polynyas (Andreas and Murphy 1986). In both hemispheres, photochemical destruction of tropospheric ozone during the polar sunrise in springtime is partially controlled by inversion strength (Oltmans et al. 1989; Barrie et al. 1988; Wessel et al. 1998). The strength of katabatic winds over the Antarctic continent and coastal regions is strongly influenced by the depth and strength of the atmospheric inversion over Antarctica (Connolley 1996). In addition, temperature changes associated with the Southern Annular Mode (SAM) and other patterns of interannual atmospheric variability are controlled by spatial variations in mean inversion strength, with stronger mean inversions associated with greater SAM influence on

surface air temperature (van den Broeke and van Lipzig 2004; van den Broeke 1998).

In the Arctic, the vertical structure of the atmosphere plays a strong role in regulating high concentrations of pollutants near the top of the inversion layer (Bridgman et al. 1989) and cloud formation, with diminished inversion strength resulting in decreased low-level and increased midlevel cloudiness (Schweiger et al. 2008). Moreover, inversion strength plays a central role in negative longwave radiation feedback mechanisms that influence the extent of temperature and sea ice changes in the Arctic in response to anthropogenic warming (Boé et al. 2009). Accurate characterization of these mechanisms is of particular importance in global climate models (GCMs) used to predict future climate. Boé et al. (2009) suggest that models used in the Intergovernmental Panel on Climate Change (IPCC) Fourth Assessment Report (AR4) generally overestimate mean inversion strength in the Arctic and, as a result, the strength of the negative longwave feedback.

Radiosonde observations show that wintertime temperature inversion maxima at both poles occur over land areas, especially Siberia and portions of the Canadian Archipelago in the north and East Antarctica in the south, where a cold land surface combines with favorable topography and generally high atmospheric pressure to produce extremely stable atmospheric conditions (Phillpot and Zillman 1970; Curry et al. 1996; Serreze et al. 1992). Direct observations over the Arctic Ocean and adjacent seas are uncommon, with temporally discontinuous data from drift stations and aircraft providing limited coverage (Vowinkel and Orvig 1970; Serreze et al. 1992; Tjernström and Graversen 2009). These limited observations suggest that wintertime inversion strength over the Arctic Ocean can be as high as 15 K, with mean inversion depth ranging from 500 to 1,500 m (Serreze et al. 1992; Curry et al. 1996; Tjernström and Graversen 2009). Radiosonde observations over ice-covered oceans around Antarctica are almost entirely absent, resulting in little knowledge of the spatial and temporal structure of inversions from in situ methods. Recently, methods using remotely sensed observations have been developed to track inversion strength and depth. Empirical relationships between radiosonde-derived inversion strength and Moderate Resolution Imaging Spectroradiometer (MODIS) images have been used to examine spatial variations in inversion strength for individual days in the Arctic and Antarctic (Liu and Key 2003). Inversion climatologies have been constructed at both poles using observations from the High Resolution Infrared Sounder (HIRS) instrument (Liu et al. 2006). Gettelman et al. (2006) demonstrate that the Atmospheric Infrared Sounder (AIRS) can successfully reconstruct relative humidity inversions over the Antarctic continent. The AIRS satellite instrument is the main source of atmospheric data for this study.

The remote sensing and in situ studies noted above reveal that inversion strength exhibits considerable spatial and temporal variability over Arctic and Antarctic oceans. The goal of this paper is to determine the principal control on this variability. Recent research suggests a link between sea ice concentration (SIC) and inversion strength (Vavrus et al. 2000; Schweiger et al. 2008; Francis et al. 2009). However, no comprehensive examination of the relationship between SIC and inversion strength has been presented to date. Spatial variability in SIC may impact mean inversion strength by regulating heat exchange between the ocean and atmosphere. Specifically, we hypothesize that high SICs are associated with reduced loss of oceanic heat to the atmosphere and hence low surface air temperatures and that the effect of high SICs dissipates with altitude, resulting in stronger inversions over high-ice areas. Here, we compare measurements of wintertime temperature inversion strength from AIRS over Arctic and Antarctic oceans with satellite-derived sea ice concentrations. The results demonstrate that sea ice concentration is likely a principal determinant of inversion strength over polar oceans in both hemispheres.

2 Data and methods

2.1 Inversion strength measurements from satellite, radiosonde, and reanalysis

The AIRS experiment, included on the NASA Aqua satellite mission, comprises co-boresited microwave and infrared nadir viewing instruments (Aumann et al. 2003). Observed radiances are inverted to yield about 200,000 daily profiles of atmospheric temperature, water vapor and trace gases, along with cloud and surface properties (Chahine et al. 2006). The validity of the temperature profiles for a wide range of geophysical states has been established by Divakarla et al. (2006). Fetzer et al. (2004) used radiosondes and model reanalyses to demonstrate that AIRS can resolve near-surface temperature inversions for warm conditions west of the subtropical continents. Gettelman et al. (2006) show that AIRS can obtain accurate temperature and water vapor retrievals in nominal 1–2 km resolution over the cold Antarctic Plateau. Here, AIRS temperatures are used to measure wintertime temperature inversion strength over the Arctic, which we define as north of 64N, and the Antarctic (south of 64S).

Past studies of high-latitude temperature inversions using the High resolution Infrared Sounder (HIRS) have used varied definitions of inversion strength, including the difference between surface air temperature and maximum air temperature below the 700 hPa level (Liu et al. 2006) and the difference in air temperature between the lowest

pressure level showing a temperature increase and the next layer where temperature decreases (Serreze et al. 1992). Because AIRS has limited vertical resolution in the lower troposphere (temperature fields are available at 1,000, 925, 850, and 700 hPa), such flexible definitions of inversion strength are impractical in this case. Instead, we use fixed definitions of inversion strength in each hemisphere for radiosonde, reanalysis, and AIRS data products. Differences in definition may cause absolute values of inversion strength in this study to vary from previous studies. In the northern hemisphere, we use the temperature difference between the 1,000 and 850 hPa pressure levels for the winter months of December, January, and February (DJF). We choose these two levels because the mean inversion height of 500–1,500 m over the Arctic Ocean found in previous studies (Curry et al. 1996; Serreze et al. 1992) approximates the mean elevation of the 850 hPa pressure level ($\sim$1,500 m). We produce a DJF inversion strength climatology using monthly AIRS inversion strengths for all points with at least 75% temporal coverage (Fig. 1c). Wintertime surface pressure climatology over much of the Southern Ocean is less than 1,000 hPa, so in the southern hemisphere we instead use the AIRS estimate of surface air temperature (SAT) for June, July, and August (JJA). SAT is linearly interpolated from the AIRS vertical temperature profile and, as a result, may exhibit systematic biases relative to radiosonde observations. However, spatial patterns in SAT in both hemispheres closely match those at 1,000 and 925 hPa. Because the principal goals of this study relate to spatial and temporal variability in inversion strength rather than the precise inversion value, results are largely insensitive to systematic bias associated with the choice of pressure level for the inversion base. At times, negative inversion strengths are possible using these definitions. In these instances, there is no detectable atmospheric inversion present and temperatures decline with increasing elevation.

To ensure accuracy, AIRS inversion strength is compared with radiosonde-derived inversion strength at 29 locations in the terrestrial Arctic and Subarctic (Figs. 1c, 3a). Observations were extracted from the NOAA Integrated Global Radiosonde Archive (IGRA) (http://www.ncdc.noaa.gov/oa/climate/igra/index.php). Observations used here are located north of 64N and provide daily temperature observations at 1,000 and 850 hPa over at least half of the wintertime AIRS observation period (December 2002–February 2008).

While radiosonde observations provide a very reliable measure of inversion strength, spatial coverage is limited, with no long-term observations available over Arctic or Antarctic oceans. Bromwich and Wang (2005) found that inversion strength computed from the National Center for Environmental Prediction (NCEP) reanalysis and European Centre for Medium-Range Weather Forecasts (ECMWF) ReAnalysis (ERA-40) products closely match radiosonde-derived wintertime inversion strength at selected locations over the Arctic Ocean, and Tjernström and Graversen (2009) confirmed this result for ERA-40. The NCEP reanalysis is available from 1948 to the present, while the ERA-40 product is available from 1957 to 2002. Here, correlation of spatial patterns in AIRS wintertime inversion strength with NCEP and ERA-40 inversion strengths provides some additional measure of the reliability of the AIRS dataset beyond isolated radiosonde locations. These reanalysis products assimilate few in situ observations in the Arctic (and even fewer in the Antarctic) and are not sufficiently reliable to use as validations of the AIRS product (Kistler et al. 2001; Uppala et al. 2005). Still, AIRS and the two reanalysis products are independent, and strong correspondence among them would lend added confidence to the accuracy of each. Below, we compare AIRS inversions with (a) a long-term NCEP inversion strength climatology (1960–1999) and (b) mean NCEP inversion strength over the 2002–2008 AIRS observation period (Figs. 1d, 2d). The AIRS record does not overlap the ERA-40 reanalysis period, so in this case we will compare climatological AIRS inversions only with the long-term ERA-40 climatology (1960–1999). The 1960–1999 interval is chosen to match global climate model (GCM) simulations, against which AIRS, NCEP, and ERA-40 inversion strengths are also compared.

2.2 Sea ice concentration data

Maps of sea ice concentration (Figs. 1a, b, 2a, b) are extracted from the Defense Meteorology Satellite Program Special Sensor Microwave Imager (SSM/I) Monthly Polar Gridded Sea Ice Concentrations, available from the National Snow and Ice Data Center (http://nsidc.org/data/nsidc-0002.html; Comiso 1990). This product provides a measure of fractional sea ice cover over the Arctic and Antarctic on 25 km polar stereographic grids and has been used extensively to examine trends in sea ice extent (e.g. Serreze et al. 2007). We directly compare spatial patterns in mean wintertime (DJF in the Arctic, JJA in the Antarctic) inversion strength and two SIC metrics derived from this product (described Sect. 3) to assess the direction and strength of sea ice/inversion relationships.

3 Quality of AIRS data

Results presented in Figs. 1c and 3a indicate that spatial variations in AIRS-derived inversion strength over Arctic and Subarctic land areas closely match those from radiosondes, with a Pearson's correlation coefficient of $r = 0.93$

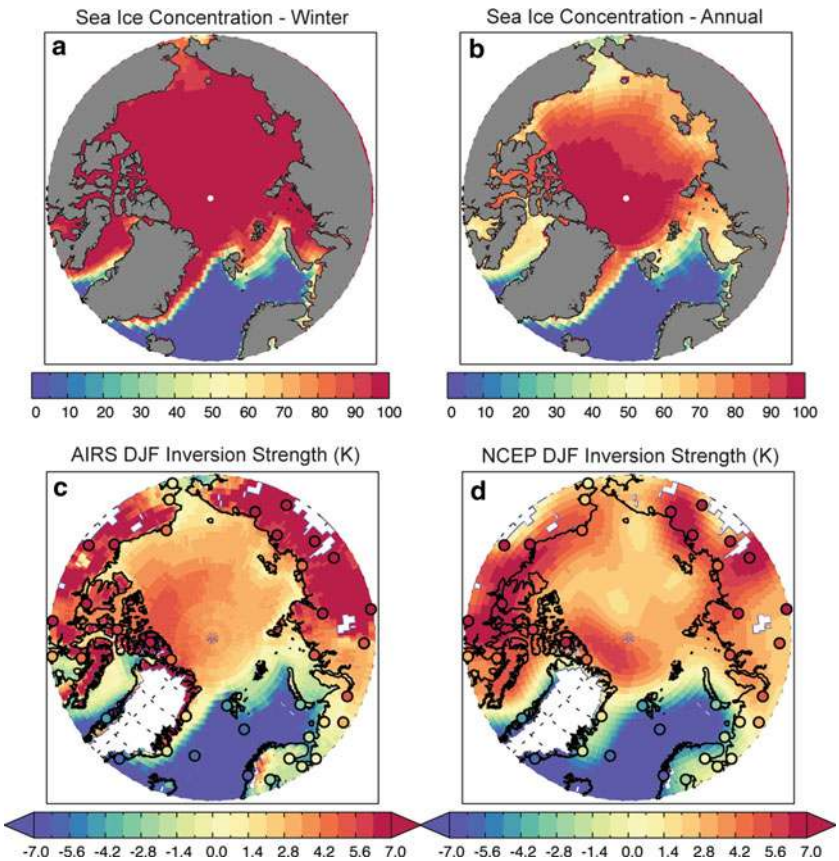

Fig. 1 **a** Mean wintertime (DJF) sea ice concentration (SIC) from SSM/I satellite data from September 2002 to February 2008, **b** mean annual SIC from SSM/I satellite data from September 2002 to February 2008, **c** mean DJF AIRS inversion strength from December 2002 to February 2008, with mean DJF inversion strength from radiosondes over the same period superimposed, **d** mean DJF NCEP reanalysis inversion strength from December 2002 to February 2008, with mean DJF inversion strength from radiosondes over the same period superimposed

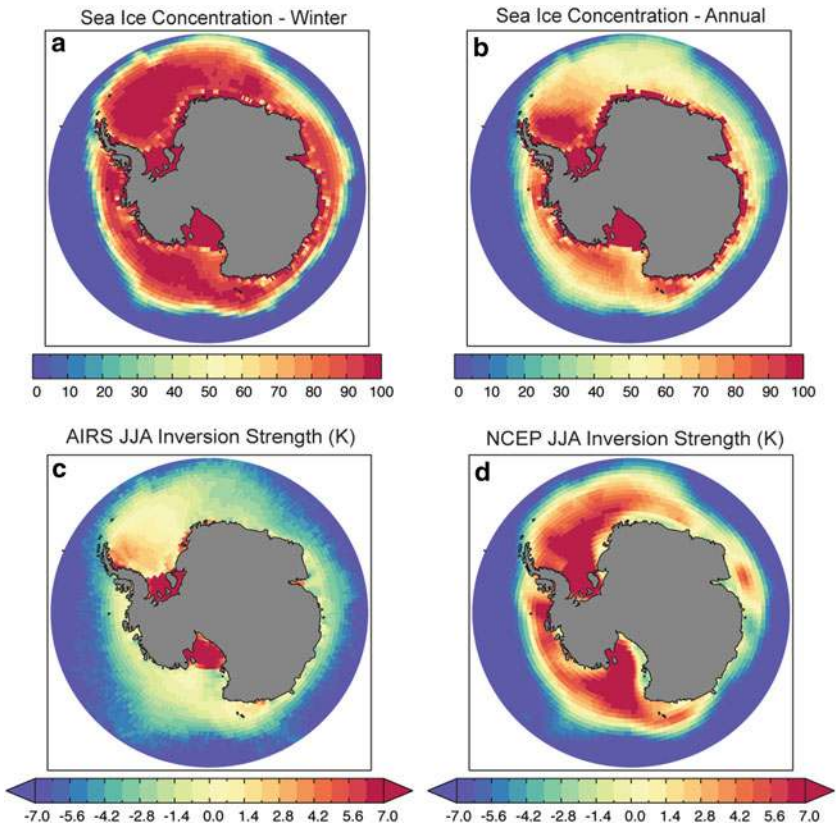

Fig. 2 **a** Mean wintertime (JJA) sea ice concentration (SIC) from SSM/I satellite data from June 2003 to August 2008, **b** mean annual SIC from SSM/I satellite data from June 2003 to August 2008, **c** mean JJA AIRS inversion strength from June 2003 to August 2008, **d** mean JJA NCEP reanalysis inversion strength from June 2003 to August 2008

($p < 0.01$) and a regression line slope of $s = 1.08$. AIRS consistently underestimates inversion strength relative to radiosonde observations by an average of 2.05 K for the 29 stations used here. A comprehensive global comparison by Divakarla et al. (2006) reveals that height-dependent bias in AIRS temperature retrieval is largest in high-latitude inland and coastal areas, precisely those locations where we compare AIRS and radiosonde inversion strength. Bias over high-latitude oceans is small by comparison (Divakarla et al. 2006), suggesting that the systematic bias seen in Fig. 3a is likely not representative of the Arctic Ocean as a whole. Radiosonde observations are extremely scarce in the Antarctic, and we do not attempt to provide separate validation for the southern hemisphere.

Spatial patterns in mean AIRS wintertime inversion strength over the entire Arctic north of 64N closely match those from the NCEP reanalysis product over the AIRS study period ($r = 0.80$, Table 1). Correlations of AIRS inversion strength with spatial patterns in the long-term NCEP ($r = 0.76$) and ERA-40 ($r = 0.75$) inversion strength climatologies over the entire Arctic are also strong. Divergence between NCEP and AIRS inversion strength is much greater over land areas than over oceans, with AIRS generally exhibiting higher inversion strengths over land areas (Fig. 3b). If Arctic Ocean areas only are considered, AIRS inversion strengths exhibit very high correlations with reanalyses ($r > 0.90$ in all cases). Mean wintertime inversion strengths over the entire northern hemisphere study area are very similar when calculated using AIRS, ERA-40, and the 2002–2008 NCEP period (Table 1). In contrast, dataset means exhibit somewhat more spread over the ocean, with AIRS showing the lowest mean inversion strength. Over the common 2002–2008 period, the difference in inversion strength between NCEP and AIRS is rather limited (roughly 1 K, which is still substantial compared to the inter-annual variability shown in Table 1). Reasons for this difference remain uncertain, although extrapolation of land-based station data to nearby ocean areas in NCEP may play some role (Fig. 1). Larger differences (<3 K) are found when comparing across time periods, but these differences may reflect actual changes in mean inversion strength between the late 20th century and 2002–2008. The long-term NCEP climatology shows the highest mean inversion strengths in both ocean-only and pan-Arctic cases, which may result from temporal inhomogeneities in the NCEP record since 1960 and differences in climate between 2002 and 2008 and the late 20th century. Because mean inversion strengths are calculated over the entire domain north of 64N in the Arctic, substantial open-ocean areas with strongly negative "inversions" are included. As such, mean inversion strength varies substantially depending on the domain selected, and the slightly negative AIRS inversion strength value stems from the inclusion of these open ocean areas. Regardless, the principal conclusion drawn from this comparison of AIRS observations with the NCEP and ERA-40 reanalyses is that the significant similarity among all products over the Arctic adds confidence to the accuracy of each.

In the Antarctic, it is not possible to compute inversion strengths over much of the continent with the definition used here because ice sheet elevation in many areas is greater than the 850 hPa pressure level. As such, we examine southern hemisphere inversion strengths only over the ocean (Fig. 2; Table 2). Spatial correlations between AIRS and reanalysis products are relatively high over the oceans in all cases, though somewhat lower than in the Arctic. This may reflect the almost complete lack of in situ observations assimilated by the reanalyses over Antarctic oceans, though, as in the Arctic, TOVS satellite-derived temperature soundings are assimilated by the NCEP and ERA-40 reanalyses over Antarctic oceans (Kistler et al. 2001; Uppala et al. 2005). Mean inversion strengths diverge substantially between ERA-40 and AIRS (Fig. 2c, low mean inversion strength) and NCEP (Fig. 2d, high inversion strength). In

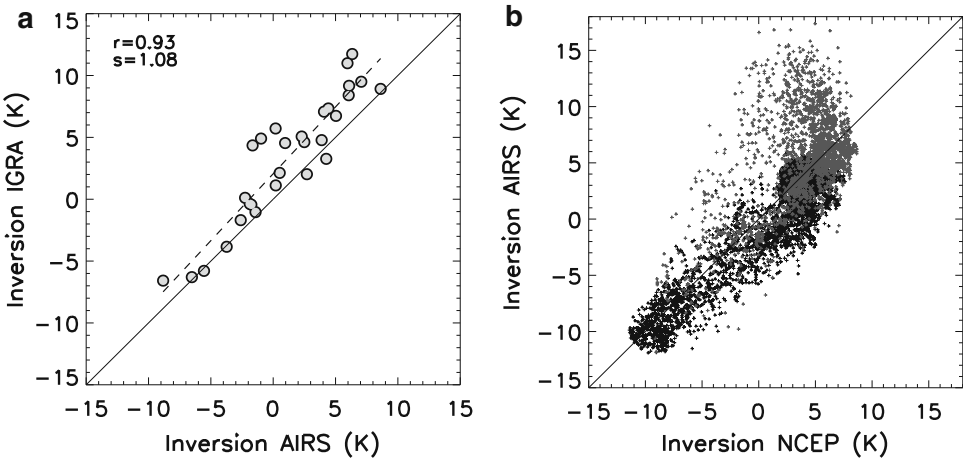

Fig. 3 **a** Scatterplot of mean AIRS inversion strength and radiosonde inversion strength at points shown in Fig. 1. Correlation is statistically significant at $p < 0.01$. **b** Scatterplot of mean DJF AIRS inversion strength versus mean DJF NCEP inversion strength for the northern hemisphere north of 64N. Land points are shown in *grey*, and ocean points are shown in *black*

Table 1 Mean inversion strength in satellite and reanalysis datasets over the entire Arctic north of 64N and only over the ocean

Dataset	Time period	Mean DJF inversion (K)	Correlation with AIRS	Mean DJF inversion (Ocean) (K)	Correlation with AIRS (Ocean)
AIRS	2002–2008	1.74	1.00	−0.52	1.00
NCEP	2002–2008	1.57	0.80	0.54	0.90
NCEP	1960–1999	2.80 (0.49)	0.75	2.26	0.92
ERA-40	1960–1999	1.53 (0.51)	0.75	1.10	0.95

Standard deviations in winter inversion strength are shown in parentheses. All correlation coefficients are statistically significant at $p < 0.01$

fact, mean NCEP inversions are stronger over Antarctic oceans than in the Arctic, which seems incongruous given the greater eddy kinetic energy in the atmosphere and lower mean annual sea ice concentration values in the Antarctic (Peixoto and Oort 1992). Since the NCEP dataset is strongly influenced by model output over Antarctic oceans (Kistler et al. 2001), we suggest that the mean AIRS inversion values are likely more reliable in this case. This conclusion is also supported by the fact that spatial patterns in ERA-40 mean wintertime inversion strength (not shown) match AIRS inversion strengths quite closely. If AIRS is correct, then the average inversion strength over Antarctic oceans south of 64S is, in fact, slightly negative. This results from the inclusion of both areas with weakly positive inversions and areas with a strongly negative atmospheric temperature gradient. The latter occur where wintertime and annual sea ice concentrations are low. AIRS is the only gridded dataset (of those examined here) based everywhere on observational data, and spatial patterns in AIRS inversions are both internally consistent and a close match with patterns in reanalysis and radiosonde inversions. As such, we have high confidence in results based on spatial and temporal patterns in the AIRS dataset.

4 Sea ice–inversion relationship

Spatial comparison of mean wintertime SIC with mean wintertime inversion strength yields very high and statistically significant positive correlations for both the Arctic (Fig. 4a, $r = 0.78$) and Antarctic (Fig. 5a, $r = 0.63$). The relationship is nonlinear in each case, however, with a substantial increase in the range of inversion strength values as SIC approaches 100%. Note that in each of these Figs data density is substantially higher at high SIC values, reflecting the fact that most polar ocean areas are nearly 100% ice-covered in winter. If we instead compare wintertime inversion strength with average annual SIC (Figs. 4b, 5b), still stronger and more linear relationships emerge in both hemispheres ($r = 0.88$ in the Arctic, 0.86 in the Antarctic). This improvement arises largely from the behavior of locations with high wintertime SIC. In the Arctic, examination of only those areas where wintertime SIC >90% (shown in red) reveals low correlations in Fig. 4a ($r = 0.22$) but a statistically significant correlation in Fig. 4b ($r = 0.71$). A similar result is evident for high SIC areas in the Antarctic in Fig. 5a ($r = 0.43$) and 5b ($r = 0.77$).

To explain these differences, we suggest that annual SIC is a surrogate for wintertime ice thickness, particularly in areas where wintertime SIC is nearly saturated. Areas with high wintertime but lower annual SIC will likely contain more extensive sub-areas of thin, first-year ice in the winter than will areas with high ice concentration in all seasons. As heat transport through first-year ice is substantially greater than through multiyear ice (Maykut 1978; Lindsay and Rothrock 1994; Schramm et al. 1997), pixels containing extensive first-year ice in the winter will have higher surface air temperatures and weaker inversions than other pixels with high wintertime ice concentrations. This interpretation is supported by a strong, though apparently nonlinear, correspondence of wintertime sea ice thickness and mean annual SIC in global climate models included in the Coupled Model Intercomparison Project 3 (CMIP3) (Fig. 6). Additionally, a comparison of Fig. 4c and d reveals that variations in Arctic SIC principally influence temperatures at the surface, as opposed to at 850 hPa, which supports our hypothesis. The strong influence of SIC on surface air temperatures over the Arctic Ocean also confirms recent findings by Liu et al. (2009). While both 1,000 and 850 hPa temperatures are strongly anticorrelated with annual SIC, the

Table 2 Mean inversion strength in satellite and reanalysis datasets over Antarctic oceans south of 64S

Dataset	Time period	Mean JJA inversion (Ocean) (K)	Correlation with AIRS (Ocean)
AIRS	2002–2008	−1.23	1.00
NCEP	2002–2008	3.25	0.73
NCEP	1960–1999	4.67 (0.91)	0.71
ERA-40	1960–1999	0.18 (0.37)	0.86

Standard deviations in winter inversion strength are shown in parentheses. All correlation coefficients are statistically significant at $p < 0.01$

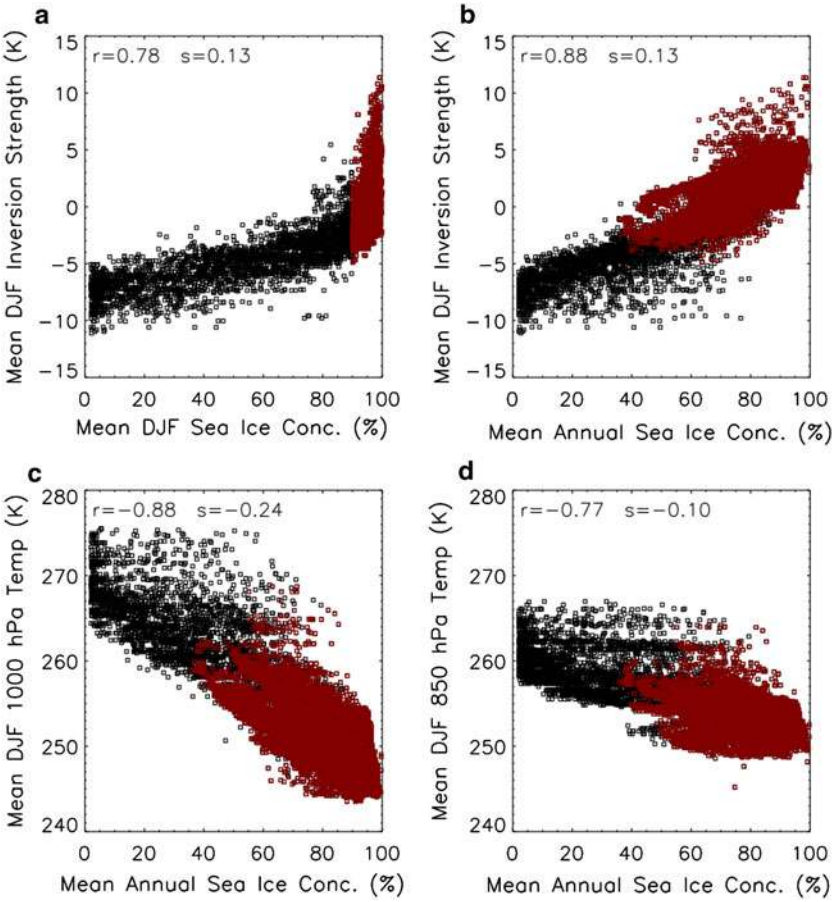

Fig. 4 Scatterplots for Arctic north of 64N between **a** mean AIRS DJF inversion strength and mean DJF sea ice concentration (SIC) from SSM/I, **b** mean AIRS DJF inversion strength and mean annual SIC, **c** mean AIRS DJF 1,000 hPa temperature and mean annual SIC, and **d** mean AIRS DJF 850 hPa temperature and mean annual SIC. Points in *red* are those points with DJF SIC >90%, which show little covariance with inversions strength in **a** but are strongly correlated with inversion strength in **b** and **c**. All correlation coefficients are statistically significant at $p < 0.01$

1,000 hPa regression slope ($s = -0.24$ K/%SIC) is more than twice the 850 hPa slope ($s = -0.10$ K/%SIC). The same phenomenon is apparent in the Antarctic (Fig. 5c, d), though the surface air temperature regression slope is somewhat lower ($s = -0.18$ K/%SIC) than in the Arctic. This slight contrast may relate to several differences between the hemispheres including stronger eddy activity in the Southern Ocean and differences in physical characteristics of the ice packs.

Though the linear ice extent/inversion strength relationships evident in the Arctic (Fig. 4b) and Antarctic (Fig. 5b) are quite strong, some scatter remains. One cause of this scatter is likely that annual SIC is an imperfect metric of the bulk thermal conductivity of the ice pack. A map of residuals from the best-fit linear regression in the Arctic (not shown) reveals spatially coherent patterns unrelated to ice concentration. In the northern hemisphere, the linear regression model overestimates inversion strength east of Greenland and underestimates it in the Canadian archipelago and over the Laptev and East Siberian Seas. These geographic patterns may be associated with large-scale atmospheric circulation and topographic influence, which past studies have shown to affect inversion strength (Vowinkel and Orvig 1970; Curry et al. 1996). Residual patterns are less spatially coherent in the southern hemisphere (not shown), though inversion strength in the Weddell Sea is slightly underestimated by the best-fit regression equation.

5 Discussion and conclusions

Based on the strong statistical relationship between SIC and mean wintertime inversion strength presented in Figs. 4 and 5, sea ice appears to be a principal driver of spatial variability in inversion strength in the high latitude oceans of both hemispheres. The hypothesis that the influence of SIC on temperature is greatest at the surface and dissipates with elevation is supported by the substantially greater regression slopes at the surface compared with 850 hPa and the positive correlations at both levels. There are several physical mechanisms that may help explain the SIC–inversion strength relationships observed here. In areas with low and moderate SIC, greater heat flux from open water compared to sea ice is likely the governing factor. Where ice cover is more continuous, the presence of leads and polynyas plays a similar role. In addition, the convection of seawater directly through brine

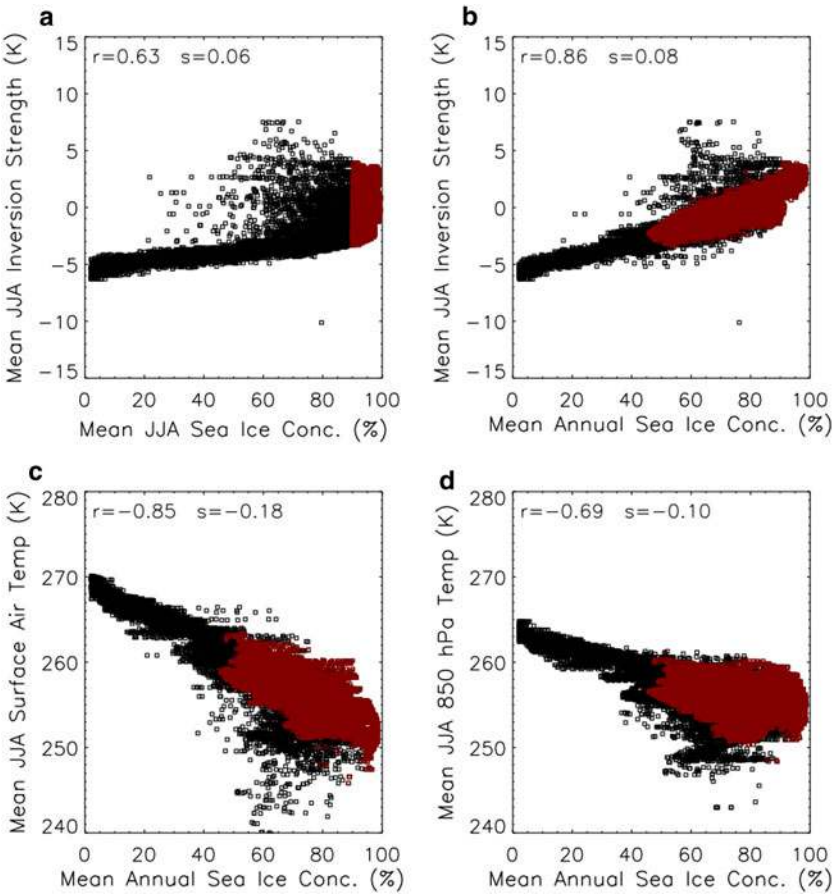

Fig. 5 Scatterplots for Antarctic south of 64S between **a** mean AIRS JJA inversion strength and mean JJA sea ice concentration (SIC) from SSM/I, **b** mean AIRS JJA inversion strength and mean annual SIC, **c** mean AIRS JJA surface air temperature temperature and mean annual SIC, and **d** mean AIRS JJA 850 hPa temperature and mean annual SIC. Points in *red* are those points with JJA SIC >90%, which show little covariance with inversions strength in **a** but are strongly correlated with inversion strength in **b** and **c**. All correlation coefficients are statistically significant at $p < 0.01$

channels in ice occurs more frequently where ice cover is thin (Lytle and Ackley 1996). As a result, those areas with high wintertime SIC that contain large areas of thin, first-year ice will likely experience greater heat flux from the ocean to the atmosphere than will areas of thick, multi-year ice. Sensible heat flux is also greater through first-year ice cover, which may reinforce this disparity (Lindsay and Rothrock 1994; Schramm et al. 1997). The influence of the latter two mechanisms is likely highest in areas where wintertime SIC is greatest, highlighted in Figs. 4 and 5 in red. Given that a higher proportion of first-year ice is likely in areas with lower mean annual SIC values, it is unsurprising that a linear relationship between mean annual SIC and mean wintertime inversion strength exists, even where wintertime SIC is nearly 100%.

It is somewhat unexpected that SIC/inversion relationships appear to be so similar in the two hemispheres given differences in atmospheric circulation patterns and ice growth and decay mechanisms. This similarity suggests that the mechanisms by which sea ice drives inversion strength may be similar in both polar oceans. However, we also find that mean inversion strength over Antarctic oceans is somewhat lower than in the Arctic. This result may stem from several differences between the hemispheres, including the southern hemisphere's lower overall mean annual SIC (SH 62%, NH 74%) and the extremely limited area of thick, multiyear ice in the Antarctic. Substantially greater eddy activity over ice-covered areas in the Antarctic than in the Arctic (Peixoto and Oort 1992) would also lower atmospheric stability.

Rapid changes in SIC and thickness recently observed over the Arctic Ocean (Serreze et al. 2007; Giles et al. 2008; Armstrong et al. 2003) suggest that mean wintertime inversion strength may be decreasing over time. The AIRS satellite record is of insufficient length to capture long-term trends, and trend analysis using reanalysis products is unreliable. Comparison of monthly area-averaged SIC with inversion strengths for December, January and February 2002–2008 ($n = 18$) yields a correlation coefficient of $r = 0.71$, suggesting that a positive temporal relationship may exist (Fig. 7a). In the southern hemisphere (Fig. 7b), we perform a similar analysis using June, July, and August 2003–2008 SICs and inversion strengths and find a similarly strong positive correlation ($r = 0.66$). A weaker mean inversion would have several important implications for polar climate in the future. High concentrations of atmospheric pollutants near the top of the Arctic inversion layer will likely decline if stability of the lower troposphere decreases. Schweiger et al. (2008) also suggest that low-level cloudiness may decrease while midlevel cloudiness

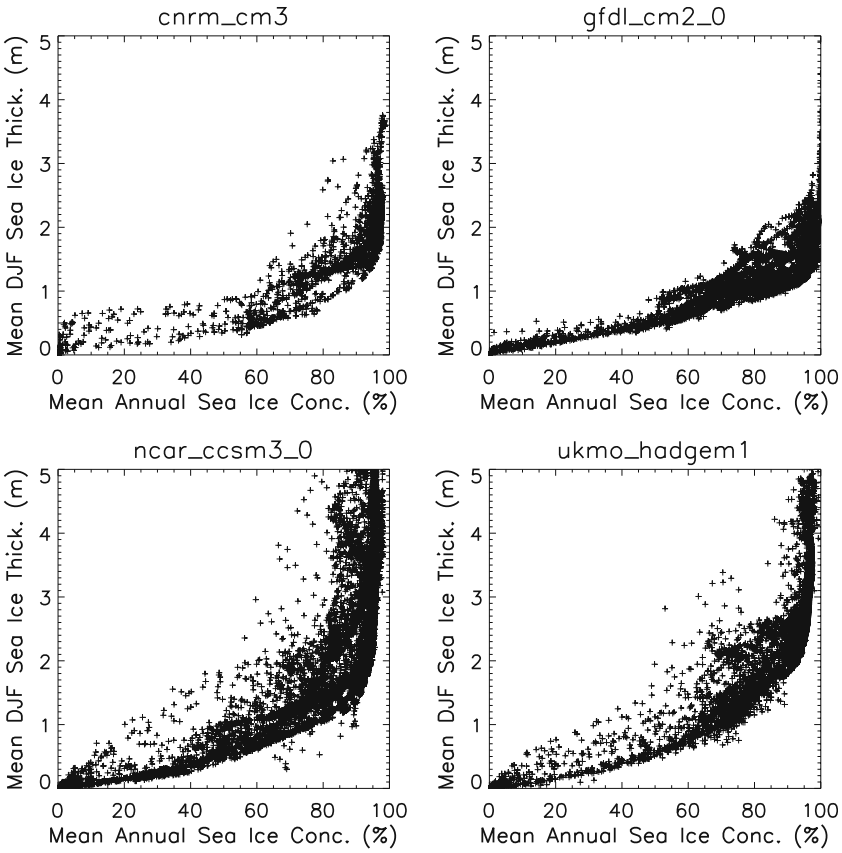

Fig. 6 scatterplots comparing mean wintertime (DJF) inversion strength with mean annual sea ice concentration over Arctic oceans for four CMIP3 model runs. Similar relationships for 13 other CMIP3 model runs are not shown

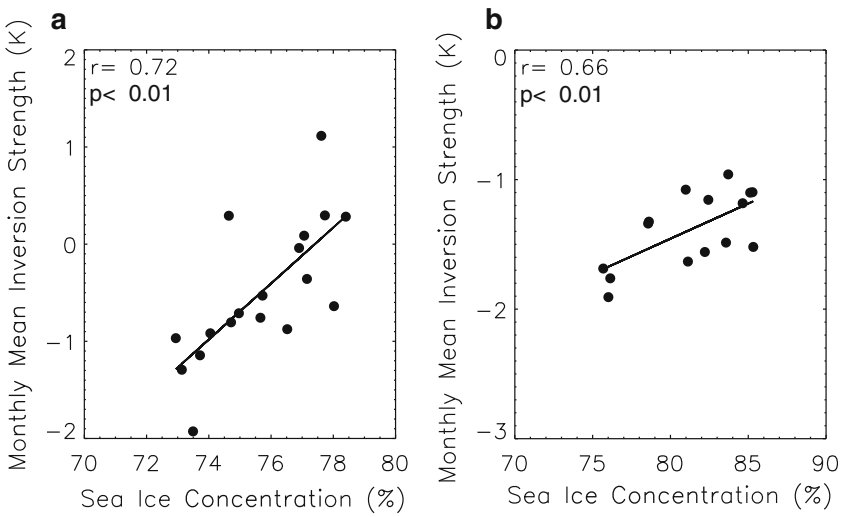

Fig. 7 Scatterplots between wintertime monthly area-averaged inversion strength and sea ice concentration for the Arctic (**a**) and Antarctic (**b**). Each point represents 1 month (DJF 2002–2008 in **a**, JJA 2003–2008 in **b**)

may increase in most areas of the Arctic, which would influence atmospheric heat and moisture transport.

Inversion strength is often poorly represented in global climate simulations (Boé et al. 2009). We compare area-averaged mean wintertime inversion strength over Arctic oceans (Fig. 8a) in 17 general circulation models included in CMIP3 with values from satellite and reanalysis datasets presented here. We find a bias towards unrealistically high inversion strength in 15 of the 17 models compared with mean AIRS inversion strength, although the temporal mismatch of the datasets suggests that AIRS may not be the ideal metric in this case. If we instead use mean 1960–1999 raw NCEP inversion strength, the strongest inversions of all observational products examined here, 8 models still overestimate inversion strength by more than 2 standard deviations in the NCEP record (Table 1), while only two models underestimate inversion strength by this amount. A comparison of NCEP and AIRS inversion strengths over

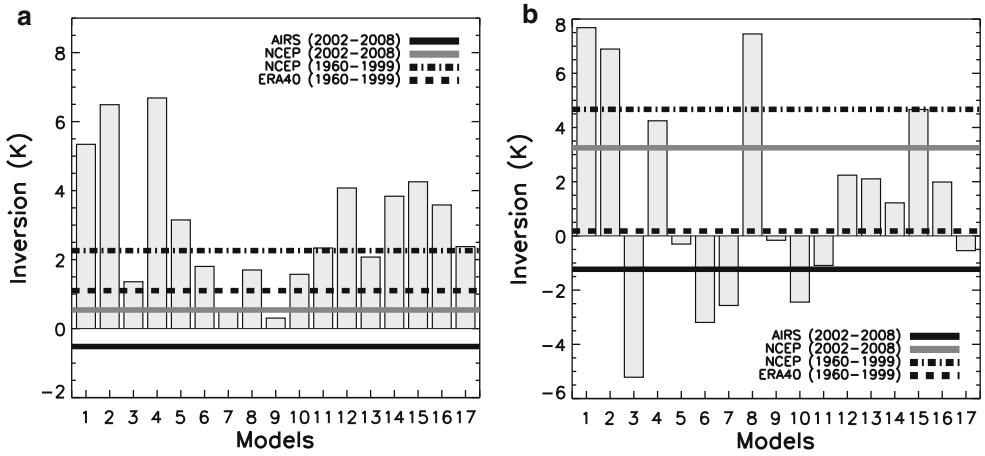

Fig. 8 Climatological strength of the inversion in the 1960–1999 period as simulated by17 CMIP3 models (Meehl et al. 2007) over **a** Arctic oceans and **b** Antarctic oceans. *Solid* and *dashed lines* indicated mean inversion strength from NCEP and ERA-40 reanalysis products and from AIRS satellite data. All the available models are used (1) cccma_cgcm3_1, (2) cccma_cgcm3_1_t63, (3) cnrm_cm3, (4) csiro_mk3_0, (5) gfdl_cm2_0, (6) gfdl_cm2_1, (7) giss_model_e_r, (8) inmcm3_0, (9) ipsl_cm4, (10) miroc3_2_medres, (11) mpi_echam5, (12) mri_cgcm2_3_2a, (13) ncar_ccsm3_0, (14) ncar_pcm1, (15) ukmo_hadgem1, (16) ukmo_hadcm3, (17) bccr_bcm2_0

the 2002–2008 period suggests that there may be a bias of roughly 1 K in NCEP. If we assume a similar bias over the 1960–1999 period then NCEP and ERA-40 inversion strengths match nearly perfectly, and 10 of the 17 models overestimate inversion strength by more than 2 standard deviations in the NCEP and ERA-40 records. Given the documented relation between climatological inversion strength and the strength of the longwave feedback parameter in the Arctic (Boé et al. 2009), it is likely that those models that overestimate inversion strength also inaccurately represent the strength of the negative longwave feedback parameter and thus underestimate the response of Arctic climate to anthropogenic forcing. The picture is less clear in the southern hemisphere (Fig. 8b), where some models show very strong mean wintertime inversions, while others show no inversions. Given the divergence in the models examined here and the likelihood that the NCEP reanalysis overestimates the mean inversion strength over Antarctic Oceans, it is likely that a substantial fraction of CMIP3 models overestimate mean inversion strength in the Antarctic. Results shown in this study suggest that to correct these errors it is worthwhile examining simulations of the sea ice–inversion relationship.

Acknowledgments This research was funded by the National Science Foundation under grants ARC-0714083 and ATM-0735056. Opinions, findings, or recommendations expressed here are those of the authors and do not necessarily reflect NSF views. We acknowledge the modeling groups, the Program for Climate Model Diagnosis and Intercomparison (PCMDI) and the WCRP's Working Group in Coupled Modeling (WGCM) for their roles in making available the WCRP CMIP3 multi-model dataset. Support for this dataset is provided by the Office of Science, U.S. Department of Energy. ECMWF ERA-40 data used in this study have been obtained from the ECMWF data server.

References

Andreas EL, Murphy B (1986) Bulk transfer coefficients for heat and momentum over leads and polynyas. J Phys Oceanogr 16:1875–1883

Armstrong AE, Tremblay LB, Mysak LA (2003) A data-model intercomparison study of Arctic sea ice variability. Clim Dyn 20:465–476. doi:10.1007/s00382-002-0284-2

Aumann HH et al (2003) AIRS/AMSU/HSB on the Aqua mission: design, science objectives, data products and processing system. IEEE Trans Geosci Remote Sens 41:253–264

Barrie LA, Bottenheim JW, Schnell RC, Crutzen RC, Rasmussen RA (1988) Ozone destruction and photochemical reactions at polar sunrise in the lower Arctic atmosphere. Nature 334:1875–1883

Boé J, Hall AD, Qu X (2009) Current GCMs' unrealistic negative feedback in the Arctic. J Clim 22:4682–4695. doi:10.1175/2009JCLI2885.1

Bridgman HA, Schnell RC, Kahl JD, Herbert GA, Joranger E (1989) A major haze event near Point Barrow, Alaska: analysis of probable source regions and transport pathways. Atmos Environ 23:2537–2549

Bromwich DH, Wang SH (2005) Evaluation of the NCEP–NCAR and ECMWF 15- and 40-Yr reanalyses using rawinsonde data from two independent arctic field experiments. Mon Wea Rev 133:3562–3578

Chahine MT et al (2006) The Atmospheric Infrared Sounder (AIRS): improving weather forecasting and providing new insights into climate. Bull Am Meteorol Soc 87:891–894. doi:10.1175/BAMS-87-7-891

Comiso J (1990, updated 2005) DMSP SSM/I daily and monthly polar gridded sea ice concentrations, 2002–2008. In Maslanik J, Stroeve J (eds) National Snow and Ice Data Center, Boulder, Colorado USA http://nsidc.org/data/nsidc-0002.html. Accessed 07 Jul 2009

Connolley WM (1996) The Antarctic temperature inversion. Int J Climatol 16:1333–1342

Curry JA, Rossow WB, Randall D, Schramm JL (1996) Overview of Arctic cloud and radiation characteristics. J Clim 9:1731–1764

Divakarla MG, Barnet CD, Goldberg MD, McMillin LM, Maddy E, Wolf W, Zhou L, Liu X (2006) Validation of Atmospheric

Infrared Sounder temperature and water vapor retrievals with matched radiosonde measurements and forecasts. J Geophys Res 111:D09S15. doi:10.1029/2005JD006116

Fetzer EJ, Teixeira J, Olsen E, Fishbein E (2004) Satellite remote sounding of atmospheric boundary layer temperature inversions over the subtropical eastern Pacific. Geophys Res Lett 31:L17102. doi:10.1029/2004GL020174

Francis JA, Chan W, Leathers DJ, Miller JR, Veron DR (2009) Winter northern hemisphere weather patterns remember summer Arctic sea-ice extent. Geophys Res Lett 36:L07503. doi:10.1029/2009GL037274

Gettelman A, Walden VP, Miloshevich LM, Roth WL, Halter B (2006) Relative humidity over Antarctica from radiosondes, satellites, and a general circulation model. J Geophys Res 111:D09S13. doi:10.1029/2005JD006636

Giles KA, Laxon SW, Ridout AL (2008) Circumpolar thinning of Arctic sea ice following the 2007 record ice extent minimum. Geophys Res Lett 35:L22502. doi:10.1029/2008GL035710

Kistler R, Kalnay E, Collins W et al (2001) The NCEP/NCAR 50-year reanalysis: monthly means CD-ROM and documentation. Bull Am Meteorol Soc 82:247–268

Lindsay RW, Rothrock DA (1994) Arctic sea ice temperature from AVHRR. J Clim 7:174–183

Liu Y, Key JR (2003) Detection and analysis of clear sky, low-level atmospheric temperature inversions with MODIS. J Atmos Ocean Technol 20:1727–1737

Liu Y, Key JR, Schweiger A, Francis J (2006) Characteristics of satellite-derived clear-sky atmospheric temperature inversion strength in the Arctic, 1980–96. J Clim 19:4902–4913

Liu Y, Key JR, Wang X (2009) Influence of changes in sea ice concentration and cloud cover on recent Arctic surface temperature trends. Geophys Res Lett 36:L20710

Lytle VI, Ackley SF (1996) Heat flux through sea ice in the western Weddell Sea: convective and conductive transfer processes. J Geophys Res 101((C4)):8853–8868

Maykut GA (1978) Energy exchange over young sea ice in the central Arctic. J Geophys Res 83((C7)):3646–3658

Meehl GA et al (2007) Global Climate Projections in Climate Change 2007: The physical Science Basis: contributions of Working Group I to the Fourth Assessment Report of the Intergovernmental Panel on Climate Change. Cambridge University Press, Cambridge, UK

Oltmans SJ, Schnell RC, Sheridan PJ, Peterson RE, Li SM, Winchester JW, Tans PP, Sturges WT, Kahl JD, Barrie LA (1989) Seasonal surface ozone and filterable bromine relationship in the high Arctic. Atmos Environ 23:2431–2441

Peixoto JP, Oort AH (1992) The physics of climate. American Institute of Physics, New York

Phillpot HR, Zillman JW (1970) The surface temperature inversion over the Antarctic Continent. J Geophys Res 75(21):4161–4169

Schramm JL, Holland MM, Curry JA, Ebert EE (1997) Modeling the thermodynamics of a sea ice thickness distribution 1. Sensitivity to ice thickness resolution. J Geophys Res 102(C10):23079–23091

Schweiger AJ, Lindsay RW, Varvus S, Francis JA (2008) Relationships between Arctic sea ice and clouds during autumn. J Clim 21:4799–4810

Serreze MC, Kahl JD, Schnell RC (1992) Low-level temperature inversions of the Eurasian Arctic and comparisons with Soviet drifting station data. J Clim 5:615–629

Serreze MC, Holland MM, Stroeve J (2007) Perspectives on the Arctic's shrinking sea-ice. Science 5818:1533–1536. doi:10.1126/science.1139426

Tjernström M, Graversen RG (2009) The vertical structure of the lower Arctic troposphere analysed from observations and the ERA-40 reanalysis. Q J R Meteorol Soc 135:431–443

Uppala SM et al (2005) The ERA-40 Reanalysis. Q J R Meteorol Soc 131:2961–3012. doi:10.1256/qj.04.176

Van den Broeke MR (1998) The semiannual oscillation and Antarctic Climate. Part 1: influence on near surface temperatures (1957–79). Antarct Sci 10(2):175–183

Van den Broeke MR, van Lipzig NMP (2004) Changes in Antarctic temperature, wind and precipitation response to the Antarctic Oscillation. Ann Glaciol 39:119–127

Vavrus S, Gallimore R, Liu Z (2000) A mixed-flux equilibrium asynchronous coupling scheme for accelerating convergence in ocean-atmosphere models. Clim Dyn 16:821–831. doi:10.1007/s003820000082

Vowinkel E, Orvig S (1970) The climate of the North Polar Basin. In: Orvig S (ed) World Survey of Climatology, vol 14, Climates of the Polar Regions. Elsevier, Amsterdam pp 129–226

Wessel S, Aoki S, Winkler P, Weller R, Herber A, Gernandt H, Schrems O (1998) Tropospheric ozone depletion in Polar Regions: a comparison of observations in the Arctic and Antarctic. Tellus 50B:34–50

Wexler H (1936) Cooling in the lower atmosphere and the structure of polar continental air. Mon Weather Rev 64(4):122–136